SEQUENTIAL SEISMIC INVERSION USING PLANE-WAVE SYNTHESIS

A DISSERTATION
SUBMITTED TO THE DEPARTMENT OF GEOPHYSICS
AND THE COMMITTEE ON GRADUATE STUDIES
OF STANFORD UNIVERSITY
IN PARTIAL FULFILLMENT OF THE REQUIREMENTS
FOR THE DEGREE OF
DOCTOR OF PHILOSOPHY

By
Jun Ji
October, 1995

printed as Stanford Exploration Project No. 90
by permission of the author

I certify that I have read this thesis and that in my opinion it is fully adequate, in scope and in quality, as a dissertation for the degree of Doctor of Philosophy.

Jon F. Claerbout (Principal Advisor)

I certify that I have read this thesis and that in my opinion it is fully adequate, in scope and in quality, as a dissertation for the degree of Doctor of Philosophy.

Biondo L. Biondi

I certify that I have read this thesis and that in my opinion it is fully adequate, in scope and in quality, as a dissertation for the degree of Doctor of Philosophy.

Norman Sleep

I certify that I have read this thesis and that in my opinion it is fully adequate, in scope and in quality, as a dissertation for the degree of Doctor of Philosophy.

Gregory Beroza

Approved for the University Committee on Graduate Studies:

Preface

All of the figures in this thesis are marked with one of three labels, [R] [NR] or [CR]. These define whether the figure is reproducible from the information provided on the CD-ROM version of this thesis.

If a figure is marked with an [R] it should be fully reproducible. All of the input data and source files required to create the figure are provided on the CD. The postscript file containing the figure can be removed and the cakefile rules provided on the CD should rebuild the figure on any of the supported computer architectures.

If a figure is marked with a [CR] it is conditionally reproducible. All the rebuild rules and source files are provided on the CD, but some particular environment or original data set may be necessary to recreate the figure. Many figures in this thesis were created using programs that use a Fortran90 compiler and run on a computer the size of Thinking Machines Co. CM-5, or Cray C90. If the code that is provided in Fortran90 will compute within a realistic time frame only on a machine like the CM-5 or Cray, then the figure will be marked as conditionally reproducible.

If a figure is marked with a [NR], it is non reproducible. It cannot be recreated from the data on the CD. The figure may have been created using a commercial software product, or software written by another author that is not available on the CD. It may be a hand drawn figure or a figure for which the commands for recreating it are not available. In all of these cases, if the reader removes the postscript file of the figure, there is no way to recreate it.

All of the reproducible and conditionally reproducible figures have a button in the caption. Clicking with the center mouse button will bring up a panel that lets one interact with the figure. One can display the figure in a separate window or destroy and rebuild the figure. If the figure is conditionally reproducible, one can view the warning message that indicates the conditions under which the figure can be rebuilt.

Sequential seismic inversion using plane-wave synthesis

Jun Ji, Ph.D.
Stanford University, 1995

ABSTRACT

The conventional inversion method for seismic data collected in areas of lateral velocity variation is performed by velocity estimation followed by reflectivity imaging. Efficient and accurate prestack depth migration plays an important role in both velocity estimation and reflectivity imaging. Plane-wave synthesis imaging is a prestack depth migration that has both efficiency and accuracy. In this thesis I develop a sequential seismic inversion method that utilizes plane-wave synthesis imaging as a major tool in both velocity estimation and angle-dependent reflectivity recovery.

For the velocity estimation, I have developed a new tomographic velocity estimation method that uses plane-wave synthesis imaging. Conventionally, reflection tomography is characterized by means of a measurement of residual moveout (RMO) that reflects traveltime errors along the ray paths where the event has moved. The method proposed in this thesis measures the RMO with the help of reflector-dependent plane-wave synthesis imaging.

The accuracy of the plane-wave synthesis in angle-dependent reflectivity recovery is obtained when the prestack data were acquired without any missing traces. In order to recover missing traces that can be found in conventional prestack data, I have developed an interpolation technique. After finding an optimum velocity spectrum of a common-midpoint gather, the missing traces are filled in by hyperbolic modeling with the optimum velocity spectrum.

The application of the sequential inversion developed in the thesis to numerically-simulated data and real data shows that the velocity estimated is accurate enough to align common-reflection point (CRP) events horizontally, and the angle-dependent reflectivity recovered shows an AVA (amplitude variation with angel) anomaly, as expected.

Approved for publication:

By ______________________________

For Department of Geophysics

Acknowledgments

I would like to thank the students, faculty and sponsors of the Stanford Exploration Project (SEP) for creating a place where exciting research ideas can be carried out. In particular, I thank my advisor, Jon Claerbout, for giving me the chance to work in an outstanding research environment. I appreciate the effort he made to provide the best computer facilities and to foster academic freedom. Francis Muir and Biondo Biondi helped me get started in my early years at SEP and I benefited from many stimulating discussions with them. Thanks go to Stew Levin, my supervisor at Mobil when I was a summer intern in 1993, for allowing me to work on the controlled illumination that initiated the work of my thesis. I would also like to thank Mobil Exploration and Production Technology Co. for access to an AVO dataset and a fruitful summer internship.

All my fellow students in the SEP made my graduate studies an enjoyable experience. I would like to thank all of them. Thanks go to Lin Zhang, Carlos Cunha-Filho, Dave Nichols, and David Lumley, who have been great discussion partners throughout the course of my study; their views have influenced me a good deal over the years. Thanks also go to Martin Karrenbach for creating a framework for an "interactive electronic document", which has become a daily-used tool. Mihai Popovici maintained not only our computer stuffs in excellent condition, but also our cheerful mood in the SEP. I am indebted to them all.

Finally, many thanks go to my parents and parents-in-law for their continuing support. Their love, support and understanding gave me the strength to complete this work. I am especially very grateful to my wife Eun Ha for her patience, understanding and encouragement, and to our son, Moon Suk, who decided to appear in our lives just when I was about to start this thesis and who served as the greatest incentive for me to graduate.

Table of Contents

List of Figures

Chapter 1

Introduction

The objective of reflection seismic techniques is the recovery of information of the subsurface with seismic soundings. In order to achieve this goal, one needs to solve an inverse problem by inferring the values of the model parameters of the subsurface from given data collected at the surface. There have been many theoretical and practical approaches to the seismic inverse problem. The primary motivation for the work developed in this thesis is the need to improve interval velocity estimation and reflectivity imaging in a practical inversion approach.

1.1 Seismic Inversion

1.1.1 Global inversion versus sequential inversion

Most of algorithms in the geophysical inverse problems can be categorized into two types: global inversion and sequential inversion. Global inversion methods are usually referred to as full waveform inversion and sequential inversion methods are mostly known as velocity estimation followed by reflectivity imaging.

Global approaches use the direct inversion approach (Tarantola, 1987). The objective function represents a measure of the difference between the recorded data, and the data predicted by a particular choice of model parameters. To be able to describe all the features in the data, the model space must assume its most complex form for the particular formulation of the forward problem. In sequential approaches the data is first reduced to a form that contains only relevant information, that is, in a formation that depends only on the subset of the model space that we want to invert for. The objective function measures only the misfit between a particular attribute of the data and the attribute predicted by a particular choice of parameters in the associated subset of the model space.

It is important to note that the data reduction involved in the sequential approach assumes that the complementary part of the model space necessary to perform the data reduction has already been estimated, also by means of an appropriate sequential approach. On the other hand, global inversion approaches make no distinction between low- and high-wavenumber components of the model. As pointed out by Claerbout (1985), this distinction is important because of the band limitation of surface seismic data. While only the low-wavenumber part of the velocity field can be reliably obtained (usually by velocity estimation), the retrieval of the reflectivity (impedance contrasts) is restricted to the high-wavenumber components. The independence between the two parts of the impedance spectrum provides a theoretical justification for the separability of the estimation process of the two parts of the model (low- and high-wavelengths). One difficulty that arises from the simultaneous inversion of the velocities and reflectivities is that whereas the effect of reflectivity perturbations can be partly linearized, the effect of velocity perturbations is highly nonlinear (Hindlet and Kolb, 1988). Another disadvantage of the direct inversion approach is its high cost; the complete physical process must be simulated at each new iteration.

1.1.2 Velocity analysis and imaging

Sequential inversion methods are performed by velocity estimation for a low-wavenumber model followed by imaging for a high-wavenumber model. Given a known background velocity, the computation of synthetic seismograms from different impedance models is a quasi-linear problem if we neglect multiple reflection and guided energy. This suggests a simplification of the original nonlinear inverse problem into a nonlinear formulation for the background velocity and, given this background, a linearized formulation for the impedance contrasts.

Many techniques for obtaining the background velocity have been proposed. A standard robust technique, normal moveout (NMO) stacking velocity analysis (Taner and Koehler, 1969), can be insufficient in complex media because of its simplified layered velocity model. Since background velocity information is contained in traveltimes, many algorithms are based on traveltime tomography, which matchs the fit between observed and calculated traveltimes. Each algorithm in tomographic velocity analysis can be characterized according to the domain it uses for traveltime picking. Conventional tomography (Bishop et al., 1985; Stork, 1988) picks the traveltime in the prestack data. In order to reduce the number, errors, and bias of picking, the semblance velocity stack panel or time-migrated section can be used for information about traveltime errors (Toldi, 1985; Fowler, 1988). The result of those two types of the time domain picking can be achieved similarly in the image domain after prestack migration by picking events for every offset (van Trier, 1990) or by picking the best residual moveout (RMO) velocity along the events in the stack images (Al-Yahya, 1987; Etgen, 1990).

After obtaining the low-wavenumber component of the velocity model by using the tomographic techniques explained above, we obtain the high-wavenumber component of the velocity model by migration which locates reflector position correctly. Conventional migration uses a simplified imaging condition that results in a zero-offset reflectivity. In order to extract more information from the seismic data, one needs to retrieve the angle-dependent reflectivity. To achieve this goal, de Bruin et al. (1990b) propose an imaging condition in the wavenumber domain after shot-profile migration using depth extrapolation (Claerbout, 1985) and Cunha Filho (1992) proposes plane-wave-response imaging after reverse time migration using time extrapolation.

1.2 Plane-wave synthesis (PWS) imaging

In this thesis I present a sequential inversion method that utilizes plane-wave synthesis imaging as a major tool in both velocity estimation and angle-dependent reflectivity recovery. Plane-wave synthesis imaging consists of two steps, wave stack and imaging of synthesized section. Wave stack that is based on the Huygens' principle synthesizes a wavefront by stacking traces over common geophone gather. The imaging of the wave-stacked section is performed like the conventional shot profile imaging (Claerbout, 1985).

In chapter 2, I show how to apply the imaging method by wavefront synthesis as well as theoretical background and some examples. In addition, I show how to construct a common incidence angle image section for a given target reflector, which provides a fundamental framework for tomographic velocity estimation (chapter 4) and angle-dependent reflectivity recovery (chapter 5).

1.2.1 History

The idea of synthesizing a line seismic source from individual shot records is not new. Imaging or processing based on wavefront synthesis has been considered since the earliest seismic exploration. Taner (1976) proposed synthesizing plane-wave sources at the surface by stacking traces in a common receiver gather. Claerbout (1976) proposed target-oriented wavefront synthesis as a robust migration scheme through regions of strong lateral velocity variation. Schultz and Claerbout (1978) presented the wave stack concept that is fundamental to the wavefront synthesis and explained how to use it for velocity analysis by synthesizing slanted plane waves. Recently, Rietveld et al. (1992) presented a successful application of the wavefront synthesis method to the well-known Marmousi data set.

1.2.2 Why plane-wave synthesis imaging ?

There are many migration algorithms that can be used for velocity estimation. Fowler (1988) used time migration, Al-Yahya (1987) used shot-profile migration, and Etgen (1990) used common-offset migration. The plane-wave synthesis imaging can be considered as a migration algorithm that takes advantages of both shot-profile and common-offset migration algorithm. In terms of accuracy, it is comparable to shot-profile migration that is known as the most accurate algorithm because it utilizes wave equation for wavefield extrapolation. In terms of efficiency, it is comparable to the common-offset imaging that produces a global subsurface image for each common-offset image section, unlike the shot-profile imaging, which produces a local image for each shot-profile image.

In addition to the favorable aspects as given above, the PWS imaging has an advantage in that it contains information about local ray trajectories on the datum where the wavefront was synthesized. This information about the ray path is not available in the algorithm that is based on the wavefield extrapolation, unless a ray tracing is additionally applied. This property motivates the development of a tomographic velocity estimation using the PWS imaging presented in this thesis.

Another advantage of the PWS imaging is the imaging condition. There are several imaging algorithms that can be used for angle-dependent reflectivity recovery. De Bruin et al. (1990b) used shot-profile migration with imaging in the Fourier domain and Cunha Filho (1992) uses the reverse-time migration with a local plane-wave-response imaging condition. Even though those methods apply the theoretically correct imaging condition, those are not practical to implement because the method of imaging in the Fourier domain requires spatial invariance of the reflectivity and the method using reverse-time migration requires to save wavefields for all the extrapolation time steps before imaging. However, the PWS imaging condition implicitly uses the same imaging condition as those and is easily applicable to a general case such as a non-flat reflector in a laterally-varying velocity medium.

1.3 An overview of the tools developed for this thesis

1.3.1 Missing-offsets interpolation

The wavefront synthesis algorithm implicitly assumes that a data set is collected with a source spacing short enough to avoid aliasing and with a large receiver cable that is long enough to avoid artifacts caused by a truncated aperture. The ideal acquisition geometry for wavefront synthesis is a fixed-split spread with an infinite aperture. In practice, however, a moving one-side spread with a finite receiver length is the typical acquisition geometry in marine surveys. The moving one-side spread acquisition leaves missing traces at near and far offsets. These missing traces cause artifacts in image from place to place according to the reflector geometry and the angle of plane wave synthesized.

If we are only interested in structural imaging, weak or broken images are not a major problem. Such image defects will disappear after the stacking of several images generated by a different plane-wave synthesis. If we are interested in angle-dependent reflectivity, however, each image from a different plane-wave needs to be analyzed separately. Therefore, the missing traces should be interpolated to produce a complete image without defects in it.

In chapter 3, I introduce an interpolation scheme for missing traces in near and far offset, which uses iteratively-reweighted, least-squares inversion.

1.3.2 Tomographic velocity estimation

Tomographic velocity inversion constitutes a nonlinear inversion problem because both the velocity and ray paths are unknown. To solve such a nonlinear problem, we use a bootstrap approach. First, starting with an initial guess and the operator based on it, we measure the traveltime errors by comparing observed traveltimes with the computed traveltimes obtained through the assumed model. Next, the error in the assumed model is solved by inverting the measured traveltime errors. We then iterate this linear inversion with the updated velocity model and hope that it converges.

If we choose the residual moveout (RMO) velocity analysis for traveltime error measure, a model-dependent RMO velocity analysis is required to compute accurate traveltime error. However, the measuring of the RMO velocity for a nonflat reflector is often difficult and is not practical to implement because it requires a line search in a prestack-migrated image cube (Zhang, 1990). To avoid such exhaustive searching, Etgen (1990) applied residual dip moveout (RDMO) before RMO velocity analysis so that the common reflection events could be lined up on the common surface location plane in the image cube.

Chapter 4 describes a way of measuring RMO velocity that reflects traveltime errors along the ray paths where the event has moved, with the help of plane-wave synthesis imaging along irregular reflectors.

1.3.3 Angle-dependent reflectivity recovery

During the past decade, the use of AVO (amplitude variation with offset) analysis in petroleum exploration has become increasingly common. Even though the goal of AVO analysis is to observe the anomalous angle-dependent reflectivity behavior of a reflector, the name *amplitude variation with offset* was chosen because most of the amplitude analysis is done in the common midpoint domain.

To analyze the properties of the reflector correctly, we need to know the angle-dependent reflectivity, which is often called AVA (*amplitude variation with angle*). When a target reflector is close to horizontal, and velocity does not change much in the lateral direction, angle-dependent reflectivity can be obtained by measuring amplitudes along the offset, followed by ray tracing for each event to determine the corresponding incidence angle to the reflector. If a target reflector has a complex structure and strong lateral velocity variation, however, AVO may not be the same as AVA because the amplitude can be affected not only by the angle-dependent reflectivity, but also by wave focusing or defocusing caused by propagation through complex velocities or structures. Resnick et al. (1987) discuss the fact that dips introduce serious problems for AVO analysis. They conclude that performing prestack migration on the data before doing AVO analysis is a necessity.

Most present day seismic migration schemes determine only the reflection coefficient of the zero offset or averaged reflectivity over a range of reflection angles for each depth point in the subsurface. This is mainly because of a simplified imaging condition. Recently, de Bruin et al. (1990b) proposed an imaging technique that produces angle-dependent reflectivity. Unfortunately, this scheme is not easy to apply when the reflector is not flat, which commonly happens in the real world.

In chapter 5, I compare the imaging conditions of three different prestack migrations in terms of angle-dependent reflectivity recovery. The imaging conditions compared are shot profile migration with the conventional imaging condition, de Bruin's imaging condition, and plane-wave synthesis imaging. The conventional imaging condition can be applied to any reflector geometry and to arbitrary velocity, but it recovers only a diagonal component of the reflectivity matrix that contains angle-dependent reflectivity information. De Bruin's imaging condition recovers a full reflectivity matrix but has difficulty in implementing for arbitrary reflector geometry and under variable velocity. Plane-wave synthesis imaging takes advantage of both conventional and de Bruin's imaging conditions. Thus, plane-wave synthesis imaging can be applied to any arbitrary structure and implicitly uses the same imaging condition as that of de Bruin.

1.4 Assumptions

Throughout this thesis, I assume that seismic wave fields recorded on the earth surface propagate through an isotropic, elastic medium. The wave fields in such a medium are vector fields consisting of the components of compressional waves (P-waves) and shear waves (S-waves). After P- and S-waves are decoupled from recorded seismic wave fields, each component honors a scalar wave equation. Therefore, I describe the imaging methods for a scalar wave field. The results can be applied to both P-waves and S-waves.

Chapter 2

Imaging by wavefront synthesis

2.1 Introduction and overview

The development of seismic stratigraphic interpretation, determination of hydrocarbon potential from amplitude measurements, delineation of reservoirs on expensive offshore tracks and etc., put rather stringent requirements for accuracy of seismic image sections. Processing seismic data by common midpoint (CMP) geometry fails to produce sections that meet the stringent requirements of present day exploration technology.

Prestack depth migration utilizes accurate wave-equation and has long been recognized as the one of the most accurate methods of imaging for areas that are geologically complicated. Another imaging method that follows the wave equation correctly without approximation is the imaging of a stack that is based on wavefront reconstruction, which is often called *controlled illumination* or *plane wave synthesis imaging.* Huygens' principle of superposition permits the synthesis of arbitrarily-shaped downward propagating wavefronts from many spherical wavefronts. The idea of synthesizing an areal seismic source from individual shot records is not new. Imaging or processing based on wavefront synthesis has been considered since 1970s. Taner (1976) proposed synthesizing plane wave sources at the surface by stacking traces in a common receiver gather. Claerbout (1976) proposed target-oriented wavefront synthesis as a robust migration scheme through regions of strong lateral velocity variation. Schultz and Claerbout (1978) presented the wave stack concept that is fundamental to the wavefront synthesis and explained how to use it for velocity analysis by synthesizing slanted plane waves. Recently, Rietveld et al. (1992) presented a successful application of the wavefront synthesis method to the well-known

Marmousi data set.

In this chapter I show how to apply the imaging method by wavefront synthesis along with the theoretical background and some examples. And I also show how to construct a common incidence angle image section for a given target reflector or for each subsurface point, which provides a fundamental framework for tomographic velocity estimation (chapter 4) and angle-dependent reflectivity recovery (chapter 5), respectively.

A well known testbed for the issues involved in prestack imaging and velocity estimation is the "Marmousi" dataset. The dataset was originally created by the Institute Français du Pétrole as a test of velocity inversion methods. It was distributed as a "blind test" dataset. The participants in the trial were given a synthetic seismic dataset and two well logs. They then attempted to invert the data to obtain a velocity model. The results of this blind test are described in Versteeg and Grau (1990).

After the blind test was complete, the true velocity model was published. The Marmousi model is a realistic model of the subsurface based on the geology of a field in offshore Angola. It has become a popular testbed for migration algorithms. Figure 2.1 shows the true Marmousi slowness model and Figure 2.2 shows a near offset section from the dataset. In this chapter, I used the Marmousi dataset as an example.

2.2 The forward model

After preprocessing for multiple reflections, the monochromatic 2-D forward model for a seismic shot record can be written as follows (Berkhout, 1985):

$$\mathbf{g}_j(z_0) = F(z_0, z_0)\mathbf{s}_j(z_0) \tag{2.1}$$

with

$$F(z_0, z_0) = \sum_{n=1}^{N} W(z_0, z_n)R(z_n)W(z_n, z_0) \tag{2.2}$$

In equation (2.1) source vector $\mathbf{s}_j(z_0)$ and measurement vector $\mathbf{g}_j(z_0)$ refer to one seismic experiment at the surface $z = z_0$ with source location at $x = x_j$. In equation (2.2), propagation operators $W(z_n, z_0)$ and $W(z_0, z_n)$ quantify the full propagation effects (down and up, respectively) between depth levels z_0 and z_n, and reflection matrix $R(z_n)$ defines the elastic angle-dependent reflection properties caused by inhomogeneities at depth level z_n. All matrices and vectors refer to one temporal Fourier component. Equations (2.1)

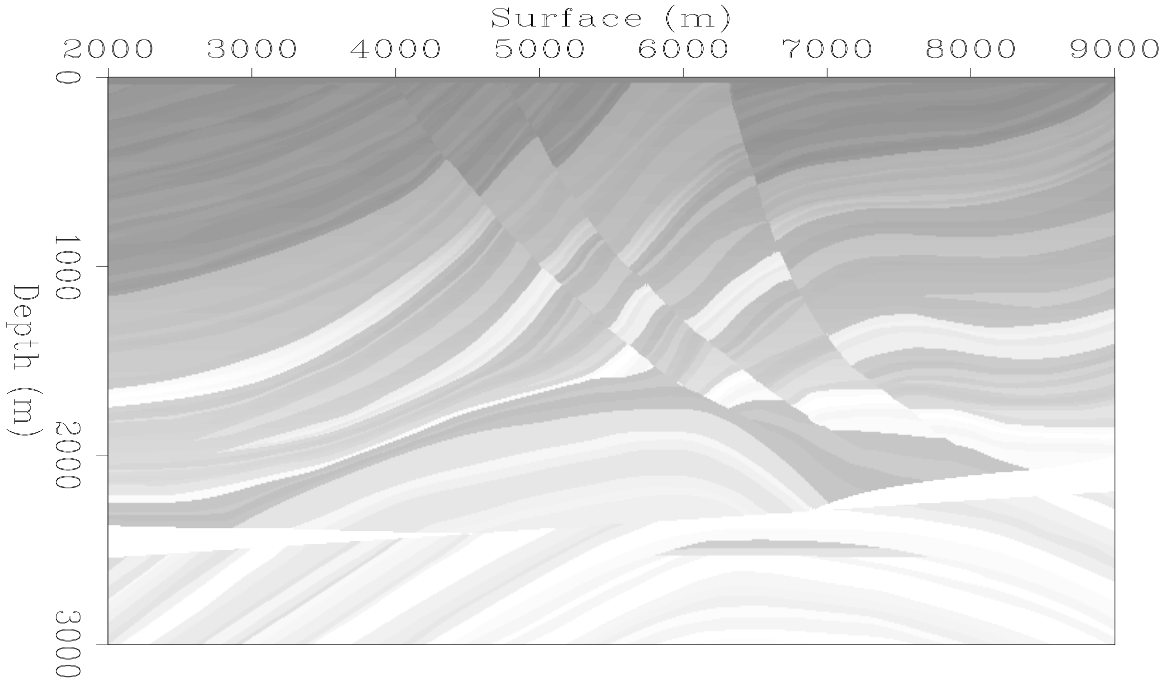

FIG. 2.1. Marmousi true velocity model. wfsyn-marm-vel [R]

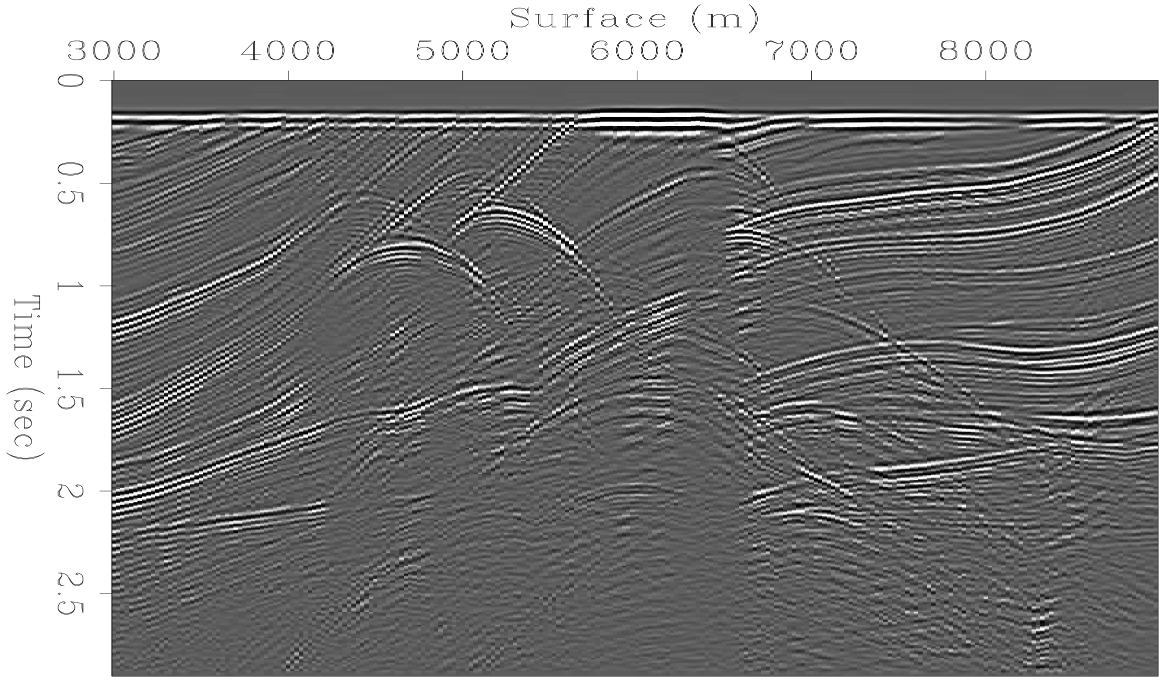

FIG. 2.2. Marmousi synthetic data, near trace section. wfsyn-marm-near [R]

and (2.2) are valid for single-component as well as for multi-component measurement of 2-D as well as 3-D data.

2.3 Wavefront synthesis using wave stacks

A *wave stack* is any stack over a common shot or geophone gather in which the moveout is independent of time (Schultz and Claerbout, 1978). It synthesizes a particular wavefront of raw data because Huygens' principle permits the synthesis of arbitrarily-shaped downward propagating wavefronts from the superposition of many spherical wavefronts. In other words, a line-source can be simulated by firing many smaller, closely-spaced point sources simultaneously or sequentially (Figure 2.3). Unlike the common midpoint stack, wave stacks have the important property of being the sampling of a wavefield and, as such, permit the treatment of formerly difficult or impossible problems with the use of the wave equation (Schultz and Claerbout, 1978).

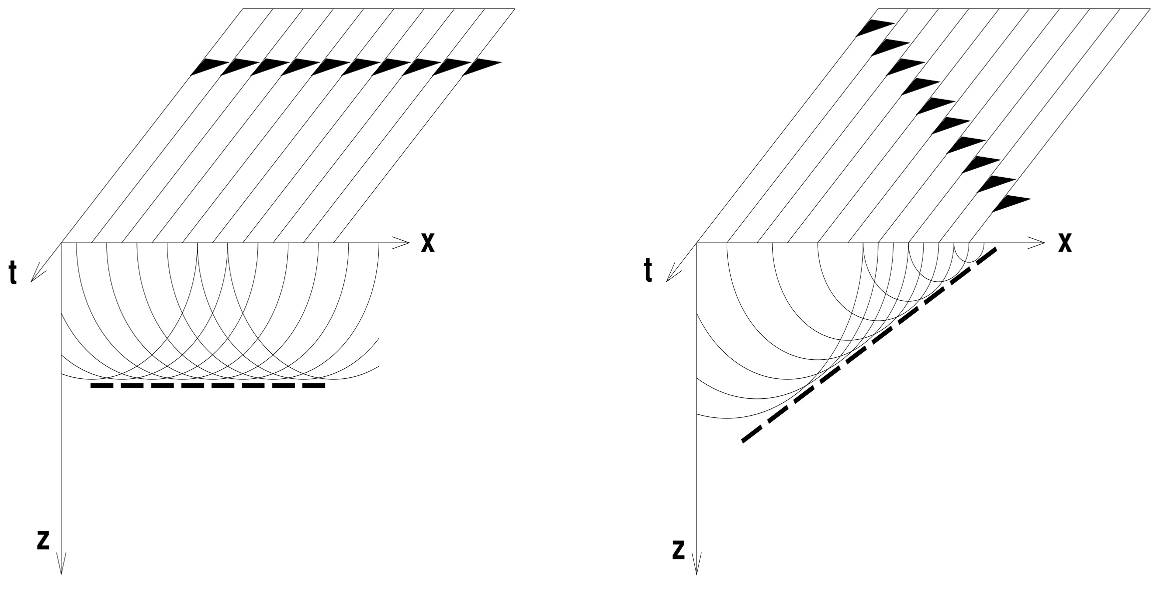

FIG. 2.3. A line source can be simulated by firing many point sources simultaneously or sequentially so as to result in a plane wavefront. wfsyn-Huygens [NR]

One of the most attractive features of the wave stack method is computational efficiency. Stacking along common geophone gathers significantly reduces the size of the data space to be migrated and produces a stacked section which has the same size as a common-offset section. Compared to shot profile migration, which requires the migration of all shot profiles to obtain a global picture of the subsurface image, the use of a wave stack considerably reduces the size of the data space to be migrated, as common-offset migration does.

Another advantage of the wave stack is that it provides a way to get an interpretable image in terms of angle-dependent reflection coefficients by controlling the incidence angle of the wavefront synthesized to a reflector.

The wave stack can be formulated by means of the linear property of the forward model operator, equation (2.1). Since the forward operator in equation (2.1) is independent of time, a linear combination of the recorded trace can be expressed by the combination of source functions as follows :

$$\sum_{j=1}^{M} \gamma_j \mathbf{g}_j(z_0) = F(z_0, z_0) \sum_{j=1}^{M} \gamma_j \mathbf{s}_j(z_0), \tag{2.3}$$

where M is the number of source functions used for wave stacking and γ_j is any complex value. The γ is called a *synthesis operator* because it synthesizes a wavefront by scaling the amplitude and shifting the phase of each source function. Therefore, we can control the wavefront by adjusting γ_j appropriately. Equation (2.3) can be simplified as

$$\bar{\mathbf{g}}(z_0) = F(z_0, z_0)\bar{\mathbf{s}}(z_0), \tag{2.4}$$

where $\bar{\mathbf{g}}(z_0)$ is called *synthesized stack* and $\bar{\mathbf{s}}(z_0)$ is the synthesis operator because it is equal to γ if we assume each shot is an impulse. The following sections explain how to determine γ_j according to the shape of the wavefront at the surface and subsurface.

2.3.1 Surface-oriented wavefront synthesis

The simplest case in wavefront synthesis is synthesizing a horizontal plane-wave source at the surface (Taner, 1976). It can be done by stacking traces along a common receiver gather and is equivalent to the wave stack equation (2.3) with γ_j equal to 1 for all j. Figure 2.4 shows this synthesis schematically.

Schultz and Claerbout (1978) have noted that reflectors of different dips can be shown more clearly by synthesizing various slanted plane waves and used the synthesis to estimate the velocity. Such a slanted plane wave synthesis is obtained by applying the wave stack equation (2.3) with

$$\gamma_j = \exp[i\omega\tau_j] \tag{2.5}$$

where

$$\tau_j = \tau_{j-1} - p\Delta x.$$

In equation (2.5), ω is the temporal frequency (recall that equation (2.3) is formulated for a monochromatic field.), τ_j is the time shifting of each source with respect to the reference source and depends on p, which is the ray parameter that controls the direction of wavefront propagation, and Δx is the interval between sources. Figure 2.5 explains schematically a simple example of the slanted wavefront synthesis.

For a more realistic example, the Marmousi data set is used. Figure 2.7 is the stacked section obtained by synthesizing a plane wave with $p = 0s/m$ at the surface (Figure 2.6) and the stacked section shown in Figure 2.9 is obtained by synthesizing a plane wave with $p = 0.0001s/m$ (Figure 2.8). The value of $p(= 0.0001s/m)$ was chosen so that the plane wavefront would have a 10 degrees incidence angle to a flat reflector whose velocity is $1700m/s$, which is the average velocity of the medium near the bottom of the water. In Figure 2.9 we can observe that some of the dipping events are enhanced and the water bottom reflection that is strong in Figure 2.7 becomes weak. In these stacked sections, we can see that the reflectors whose dip is normal to the direction of the wavefront propagation are more clearly visible than the others, respectively.

2.3.2 Target-oriented wavefront synthesis

If the reflector we are interested in is not flat or if the velocity of the overburden medium has strong lateral variation, the surface-oriented wavefront synthesis does not produce a stack that has equally strong amplitude along the reflection from the reflector. The irregular amplitude of the reflected wavefield can be explained by the wavefront distortion resulting from the strong lateral velocity change or the variation of the incidence angle of the wavefront to the reflector from place to place.

Therefore, clear illumination of reflectors that are nonflat or located under a complex velocity overburden require target-oriented wavefront synthesis (Claerbout, 1976; Schultz and Claerbout, 1978; Rietveld et al., 1992). In other words, we need a synthesis operator whose wavefront is a plane at a certain depth or along an irregular reflector, not at the surface. Using the property of the wavefield extrapolation operator that is close to unitary, we can easily generate a synthesis operator for a wave stack whose wavefront has a predefined shape at a certain subsurface location.

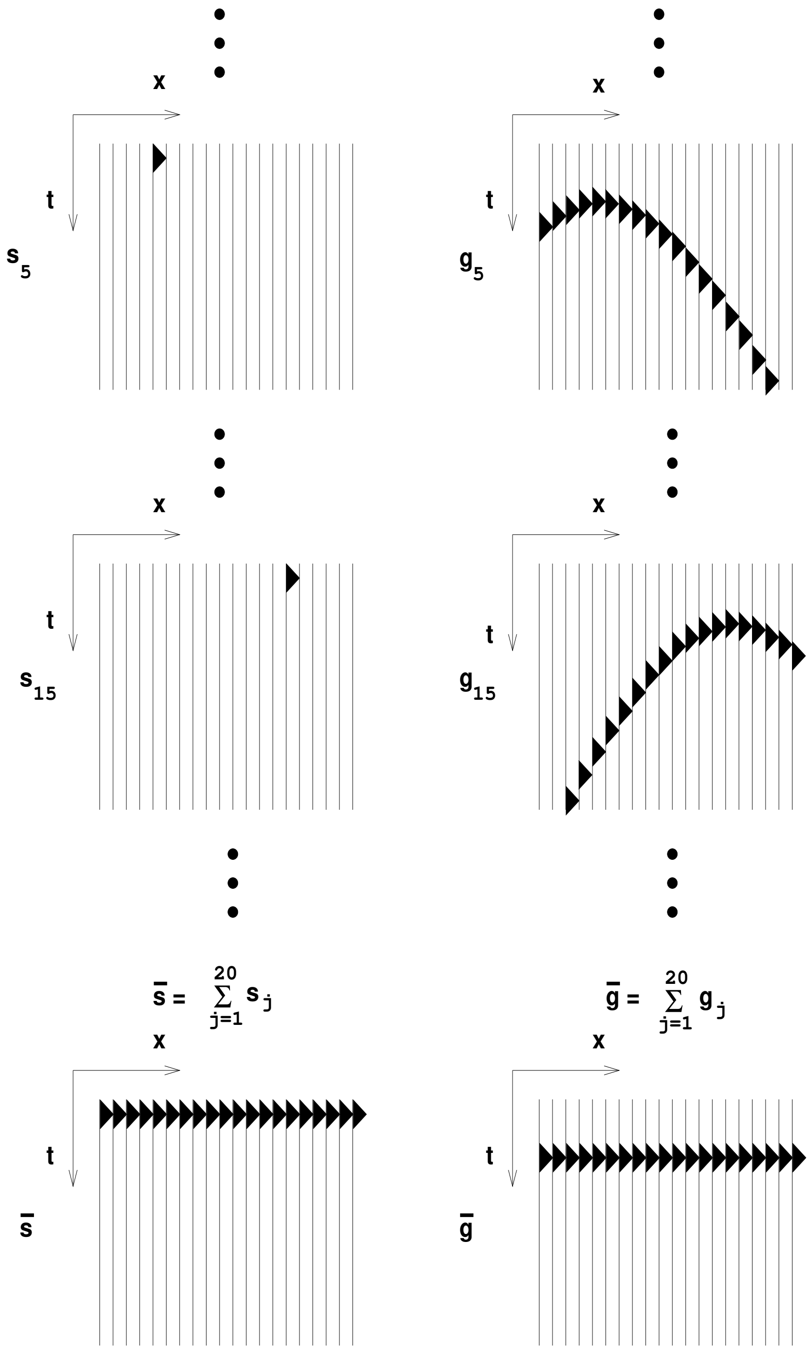

FIG. 2.4. A plane-wave synthesis at the surface. wfsyn-syn-plane-0 [NR]

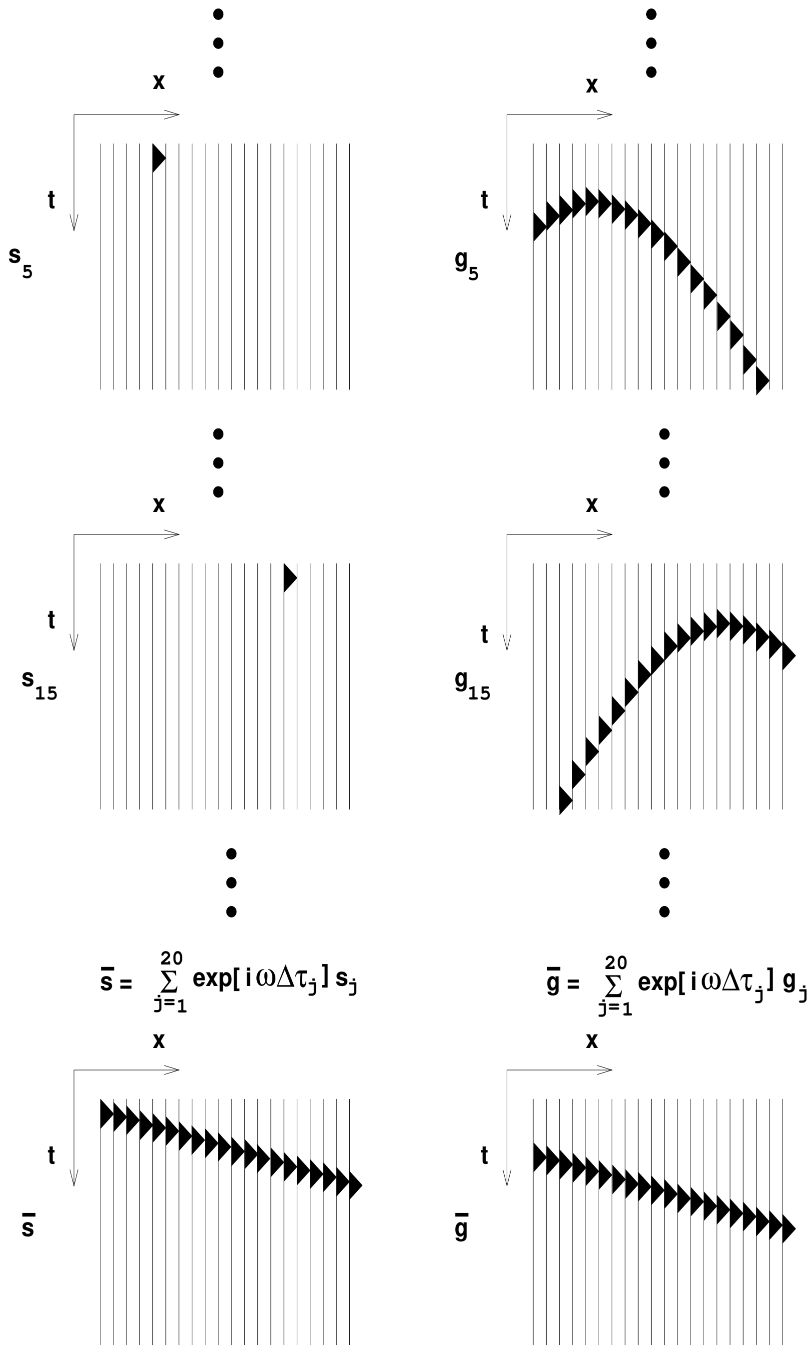

FIG. 2.5. A slanted plane-wave synthesis at the surface. wfsyn-syn-plane-1 [NR]

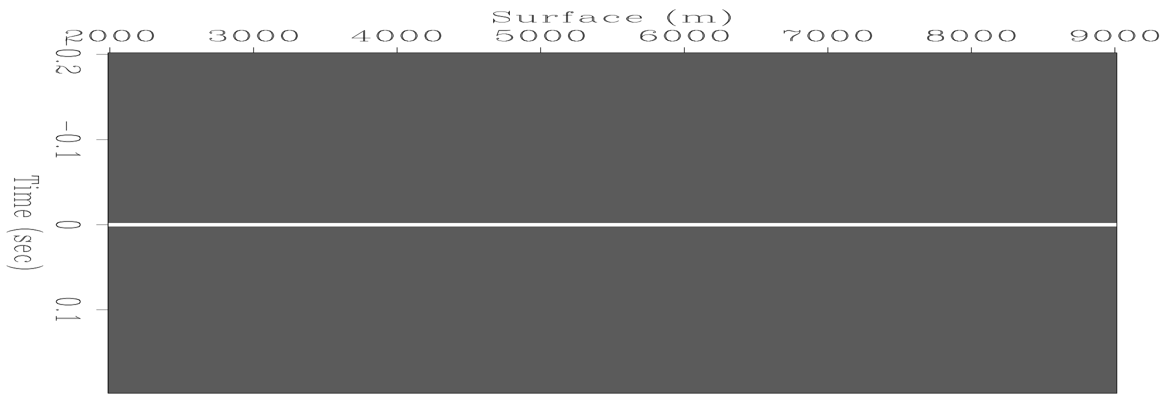

FIG. 2.6. Synthesis operator to synthesize a plane-wave with $p = 0(s/m)$ at surface. wfsyn-marm-syn-pln-0 [CR]

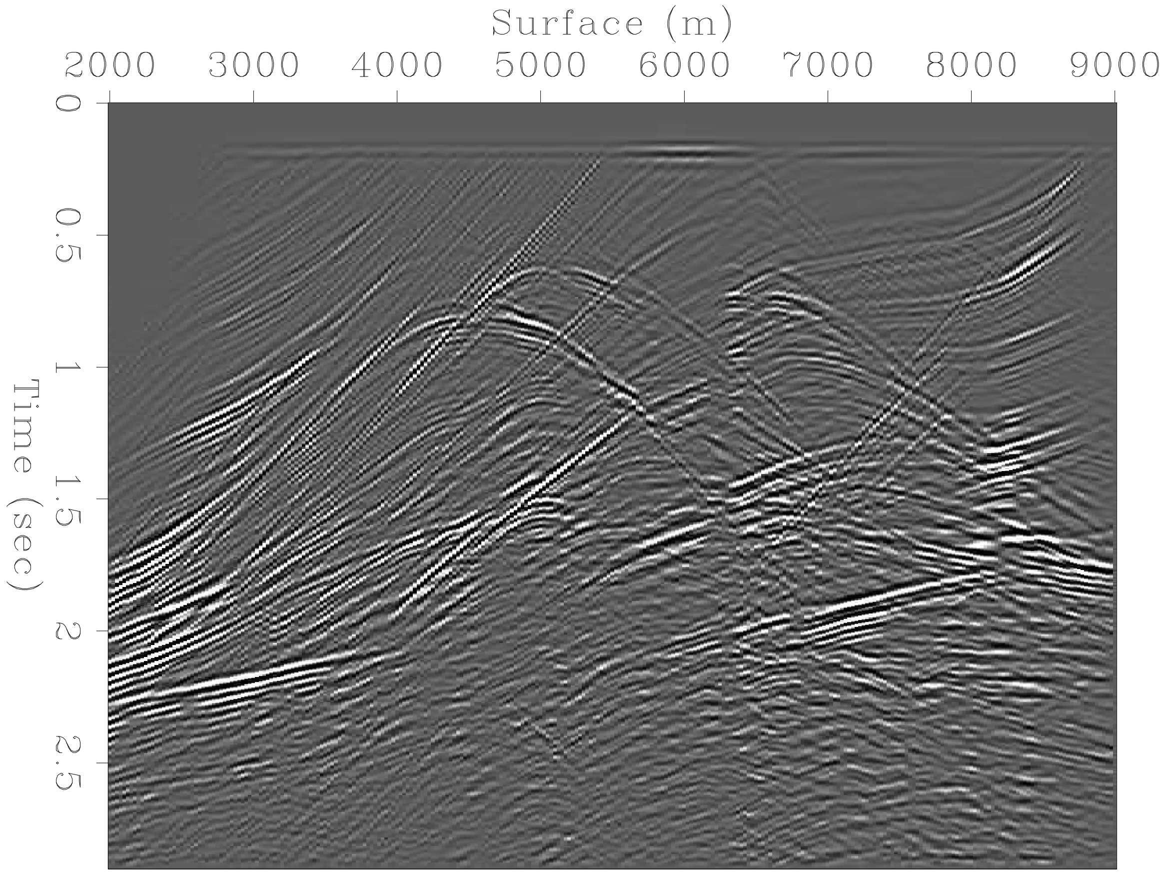

FIG. 2.7. Wave stacked section of Marmousi data set with synthesis operator shown in Figure 2.6. wfsyn-marm-stk-pln-0 [CR]

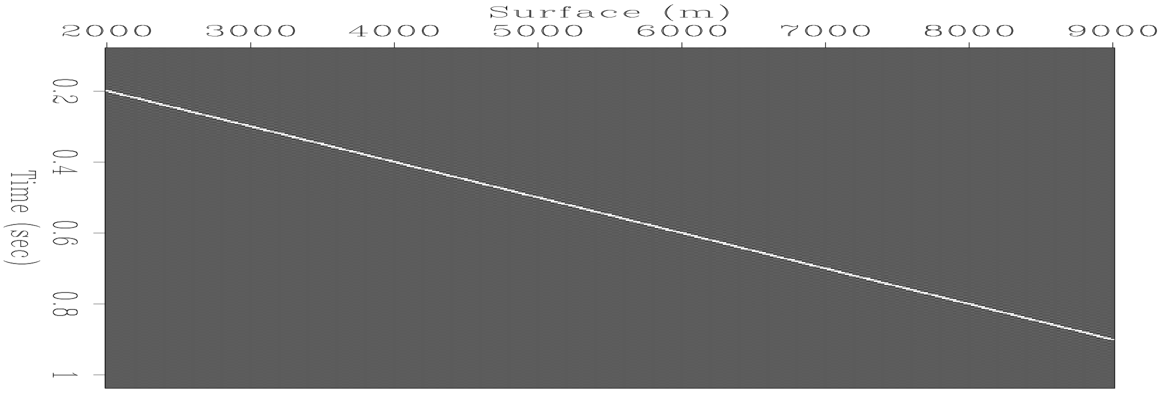

FIG. 2.8. Synthesis operator that synthesizes a plane-wave with $p = .0001(s/m)$ at surface. wfsyn-marm-syn-pos-0 [CR]

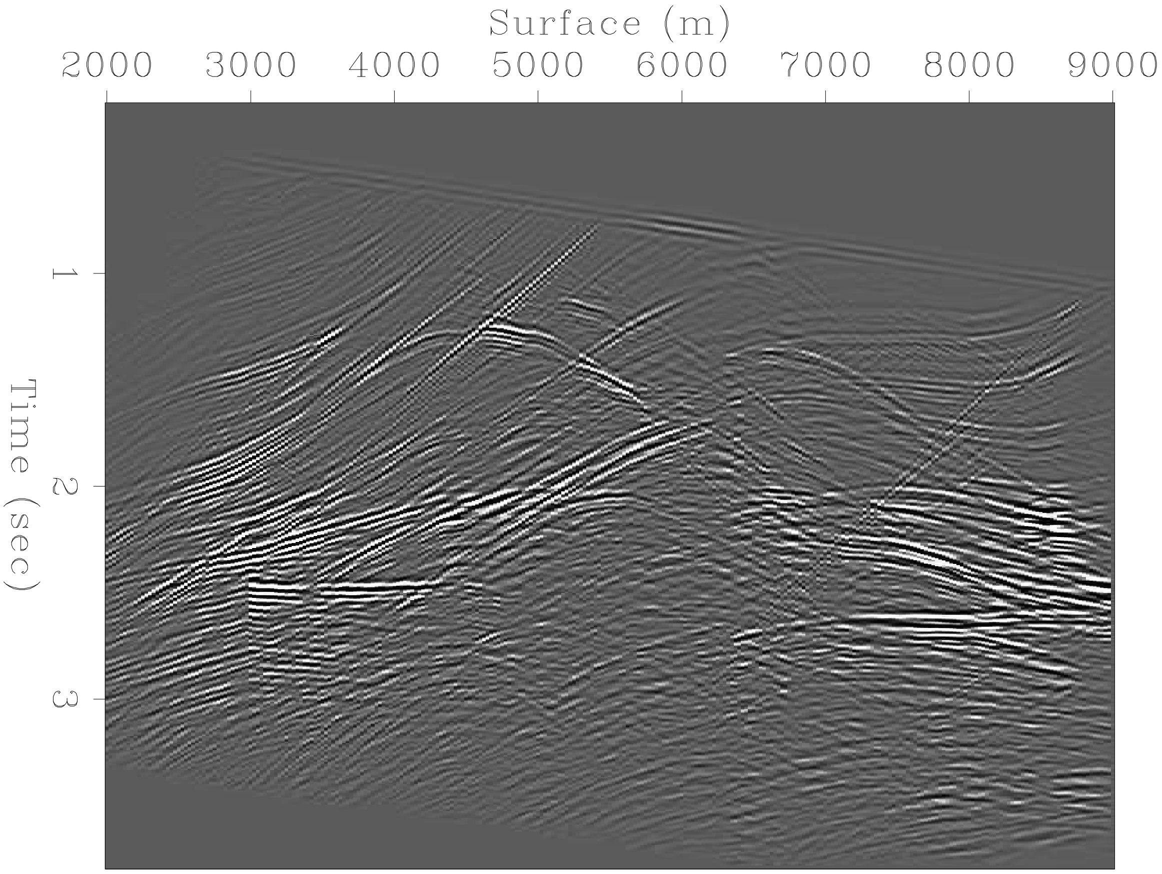

FIG. 2.9. Wave-stacked section of Marmousi data set with synthesis operator shown in Figure 2.8. wfsyn-marm-stk-pos-0 [CR]

Suppose that we want to have a downgoing wavefield $\bar{\mathbf{s}}(z_n)$ at a depth level z_n. This wavefield can be obtained by propagating a wavefield at the surface, $\bar{\mathbf{s}}(z_0)$, to the depth level z_n, as follows:

$$\bar{\mathbf{s}}(z_n) = W(z_n, z_0)\bar{\mathbf{s}}(z_0), \tag{2.6}$$

where $W(z_n, z_0)$ represents a wave propagation operator from z_0 to z_n in forward time. If we assume the propagation operator, $W(z_n, z_0)$, is a unitary operator, $\bar{\mathbf{s}}(z_0)$ can be obtained by applying the adjoint operator to both sides of the above equation as follows:

$$\begin{aligned} W^*(z_0, z_n)\bar{\mathbf{s}}(z_n) &= W^*(z_0, z_n)W(z_n, z_0)\bar{\mathbf{s}}(z_0) \\ &= \bar{\mathbf{s}}(z_0) \end{aligned} \tag{2.7}$$

where $W^*(z_0, z_n)$ is the adjoint to $W(z_n, z_0)$, which represents a wave propagation operator from z_n to z_0 and backward in time. Even though it is a widely accepted fact that wavefield extrapolation is a pseudounitary operator, the closeness to the unitary property of the extrapolation operator is different depending on the algorithm chosen in implementation. For this thesis, I used the split-step Fourier method (Stoffa and Fokkema, 1990) for the wavefield extrapolation; the pseudounitary property of the split-step Fourier extrapolation is demonstrated in Appendix A.

Assuming that every shot wavefield, $\mathbf{s}_j(z_0)$, is an impulse source at x_j, the wavefield $\bar{\mathbf{s}}(z_0)$ obtained from equation (2.7) becomes the synthesis operator

$$\gamma = \bar{\mathbf{s}}(z_0). \tag{2.8}$$

Therefore, the target-oriented wavefront synthesis is obtained by applying the wave stack equation (2.3) with γ given above.

For synthesizing a slanted wavefront at a certain depth, we only need to start with a slanted plane wave such as $\bar{\mathbf{s}}(z_n)$ in equation (2.7); that is

$$\bar{s}_j(z_n) = \exp[i\omega\tau_j]$$

Figure 2.11 is the stacked section obtained by synthesizing a plane wave with $p = 0.(s/m)$ at $1200m$ depth (Figure 2.10) and Figure 2.13 is obtained by synthesizing a plane wave with $p = 0.0001(s/m)$ (Figure 2.12). In Figures 2.11 and 2.13 we can observe that some events that were not visible in Figures 2.7 and 2.9 are now visible.

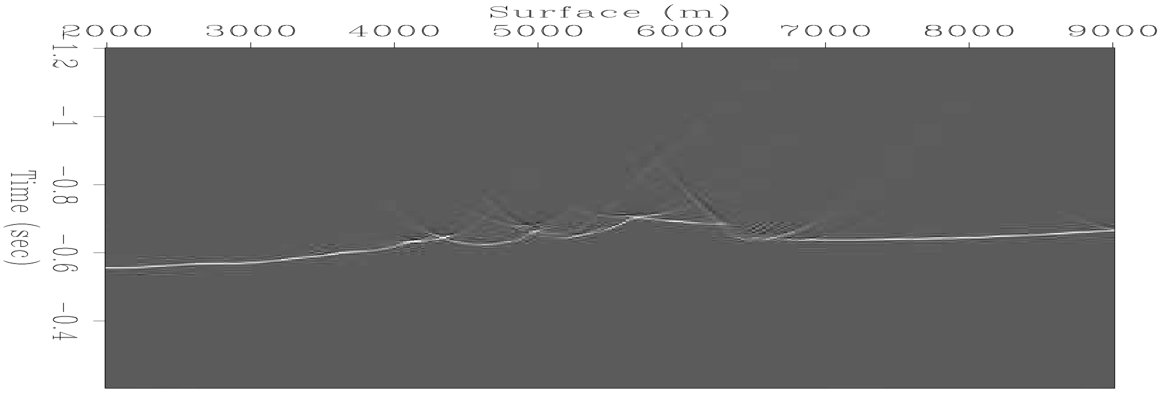

FIG. 2.10. Synthesis operator that synthesizes a plane-wave with $p = 0(s/m)$ at $1200m$ depth. wfsyn-marm-syn-pln-1 [CR]

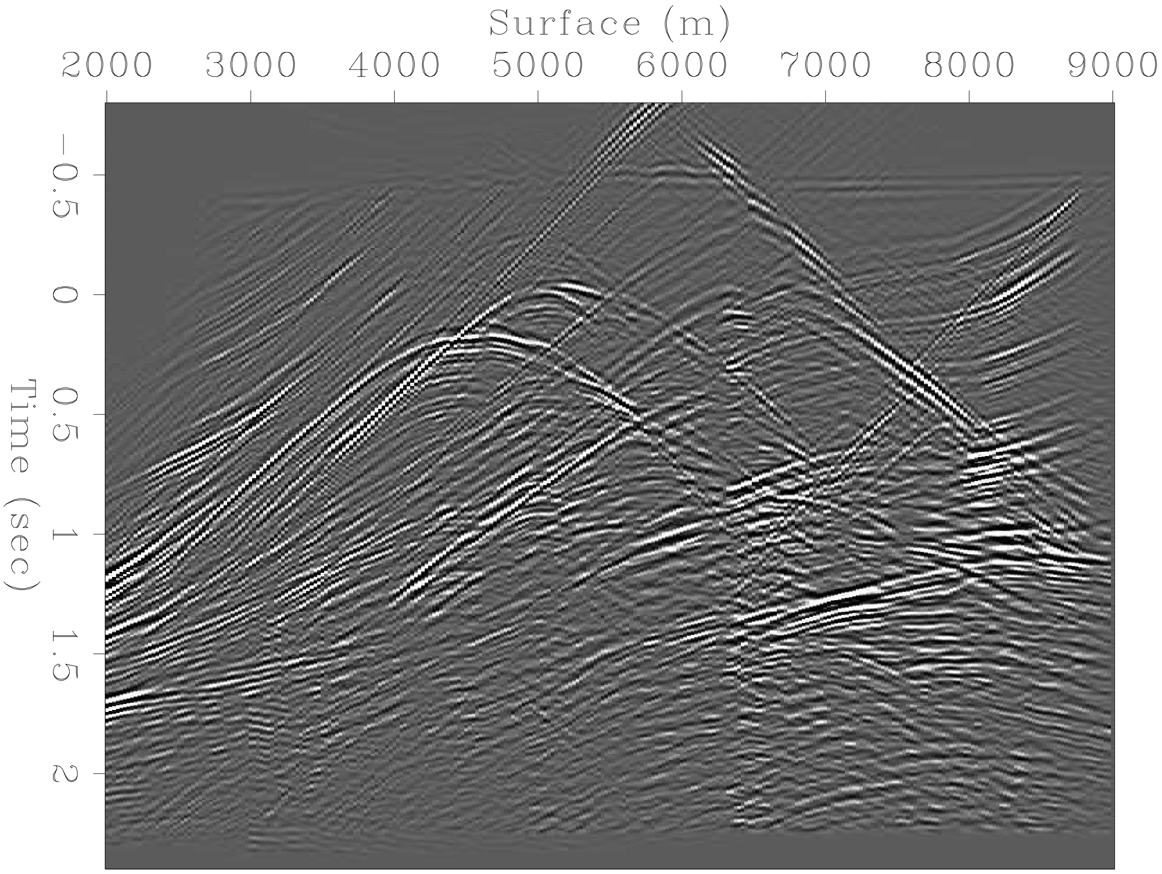

FIG. 2.11. Wave-stacked section of Marmousi data set with synthesis operator shown in Figure 2.10. wfsyn-marm-stk-pln-1 [CR]

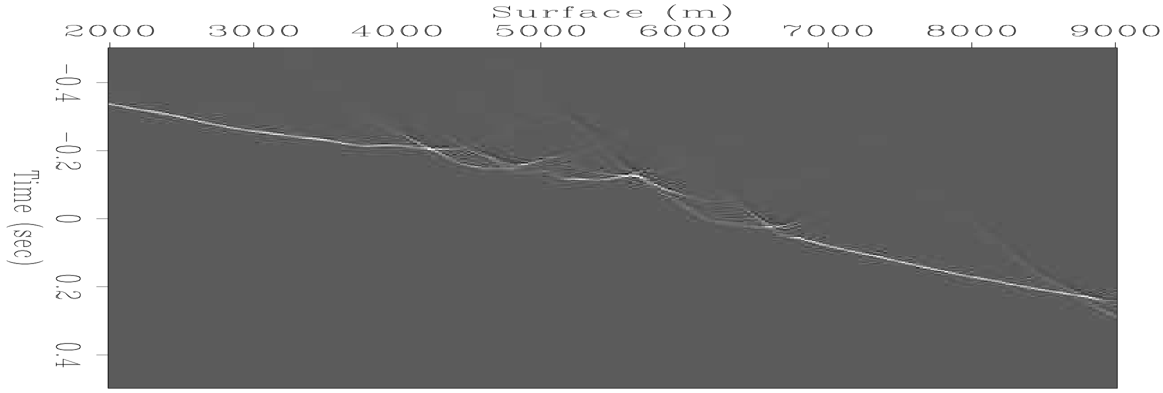

FIG. 2.12. Synthesis operator that synthesizes a plane-wave with p = .0001(s/m) at 1200m depth. wfsyn-marm-syn-pos-1 [CR]

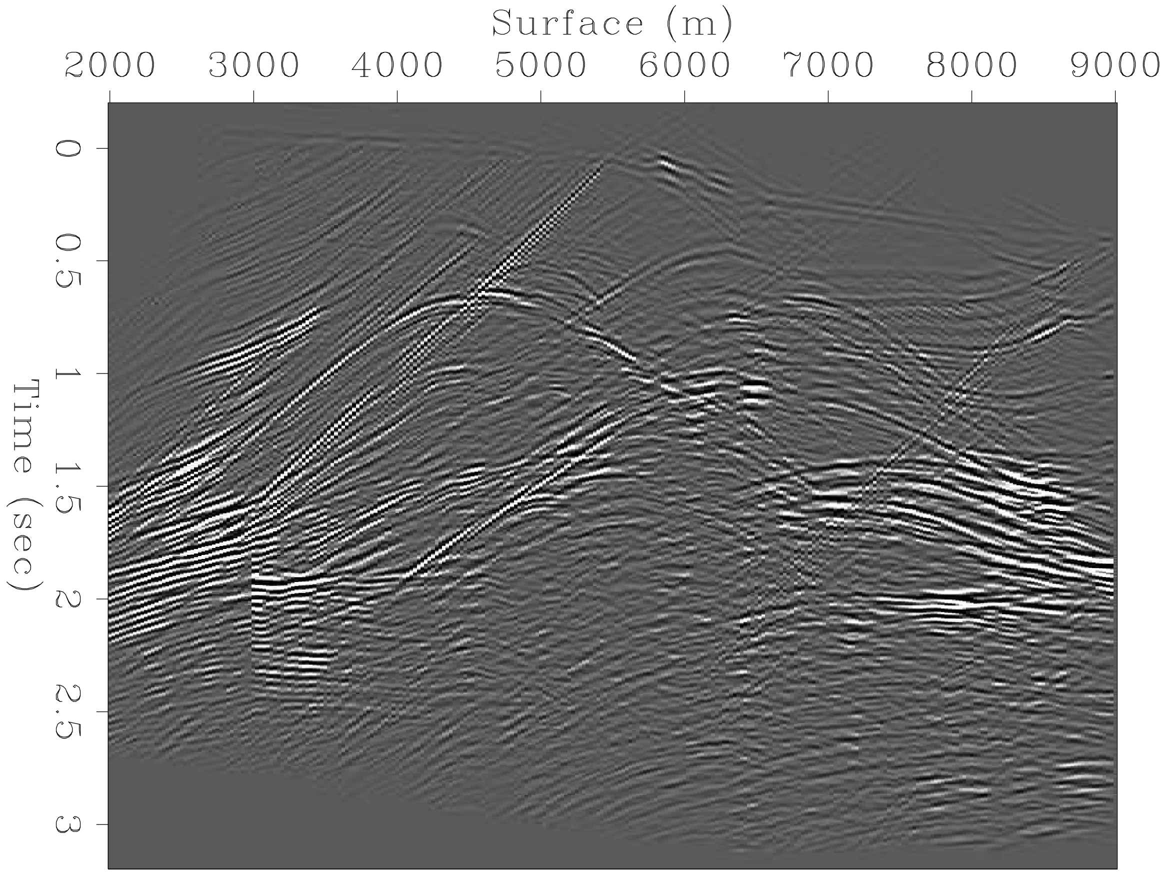

FIG. 2.13. Wave-stacked section of Marmousi data set with synthesis operator shown in Figure 2.12. wfsyn-marm-stk-pos-1 [CR]

2.3.3 Wavefront synthesis along an irregular surface

So far I have described plane wave synthesis along a flat datum either at the surface or at a depth level. In order to synthesize a plane-wave along an irregular datum, we need an extrapolation algorithm that extrapolates wavefield from an irregular datum. Suppose that we want to have a downgoing wavefield $\bar{\mathtt{s}}(r)$ along an irregular reflector $r = z(x)$. This wavefield can be obtained by propagating a certain wavefield at the surface, $\bar{\mathtt{s}}(z_0)$, to the irregular reflector $r = z(x)$, as follows:

$$\bar{\mathtt{s}}(r) = W(r, z_0)\bar{\mathtt{s}}(z_0), \tag{2.9}$$

where $W(r, z_0)$ represents a wave propagation operator from z_0 to r in forward time. If we assume the propagation operator, $W(r, z_0)$, is an unitary operator, $\bar{\mathtt{s}}(z_0)$ can be obtained by applying the adjoint operator to both sides of the above equation:

$$\begin{aligned} W^*(z_0, r)\bar{\mathtt{s}}(r) &= W^*(z_0, r)W(r, z_0)\bar{\mathtt{s}}(z_0) \\ &= \bar{\mathtt{s}}(z_0) \end{aligned} \tag{2.10}$$

where $W^*(z_0, r)$ is the adjoint to $W(r, z_0)$, which represents a wave propagation operator from r to z_0 and backward in time. Then the wavefield obtained by equation (2.10) becomes the synthesis operator, as explained in the previous section.

Therefore, to synthesize a plane-wave along an irregular reflector, we need to formulate the wavefield extrapolation from a flat surface to an irregular surface as a forward operator, $W(r, z_0)$, and find its adjoint,$W^*(z_0, r)$. Those extrapolations are formulated by modifying a standard depth extrapolation operator and are explained in Appendix B.

Another case that requires an extrapolation similar to that described above is one in which we synthesize a plane-wave at a depth level using shot gathers collected along a nonflat surface. In this case, we need to define the forward operator as an extrapolation from a flat datum to an irregular datum, $W(z_n, r)$, and as well as define its adjoint operator, $W^*(r, z_n)$. These operators are easily derived by a modification of the algorithm shown above in this section.

2.3.4 Controlling incidence angle

In the previous sections the slanted wavefront was synthesized by using the ray parameter p. If the reflector in the subsurface is generally gentle and the lateral velocity change is small, the slanted wavefronts with constant ray parameters are enough to retrieve the angle-dependent reflectivity. However, if the reflector in the subsurface has a complex structure or the lateral velocity change is not small, a slanted wavefront with a constant ray parameter is not enough to retrieve the angle-dependent reflectivity because one need to calculate the incidence angle using the velocity of the subsurface location, which corresponds to the ray parameter of the subsurface location. We then need a plane-wave with a constant-incidence angle to reflectors instead.

In order to synthesize an areal shot record for a slanted wavefront with a constant-incidence angle at a depth level, the impulse in each trace of the predefined wavefield, $\bar{\mathbf{s}}(z_n)$, must have time lag, $\Delta\tau_j$, with respect to every other trace. If the trace interval is Δx

$$\Delta\tau_j = \pm\frac{\Delta x}{v_h}, \tag{2.11}$$

where v_h is the horizontal phase velocity of the propagating wavefront at depth level z_n. Snell's law states that for a stratified earth

$$p = \frac{\sin(\theta(z))}{v(z)} = \frac{1}{v_h} = \text{constant}, \tag{2.12}$$

where p is the ray parameter, and $v(z)$ is the depth-dependent velocity of the medium. Combining equations (2.11) and (2.12), we can obtain the time lag, $\Delta\tau_j$, between the traces to simulate a plane-wave which has a constant incidence angle to the depth level as shown below:

$$\Delta\tau_j = \frac{\Delta x \sin(\theta)}{v(z_n, x_j)}. \tag{2.13}$$

Now the synthesized wavefront becomes

$$\bar{s}_j(z_n) = \exp[i\omega\tau_j]$$

with

$$\tau_j = \tau_{j-1} - \frac{\Delta x \sin(\theta)}{v(z_n, x_j)}.$$

The sign convention of the angle, θ, for the slanted wavefront used in this thesis is shown in Figure 2.16. Figure 2.15 is the stacked section obtained by synthesizing a plane wave with 10 degrees of incidence angle at 1200m depth (Figure 2.14). It looks very similar to the synthesized stack with a constant ray parameter (Figure 2.13) at the same depth level, but the difference between them becomes clear in the images shown in Figures 2.20 and 2.21. The image obtained by synthesizing a constant incidence angle

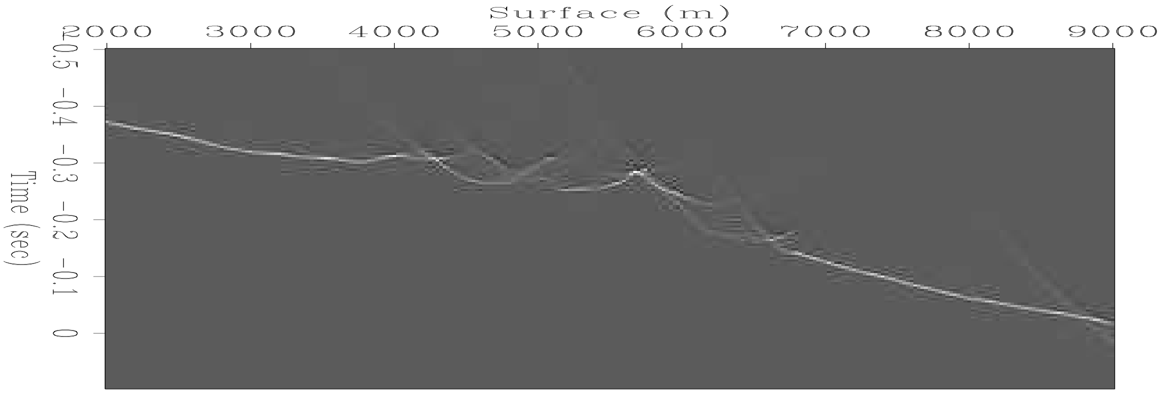

FIG. 2.14. Synthesis operator that synthesizes a plane-wave with 10 degrees angle at 1200m depth. wfsyn-marm-syn-pos-2 [CR]

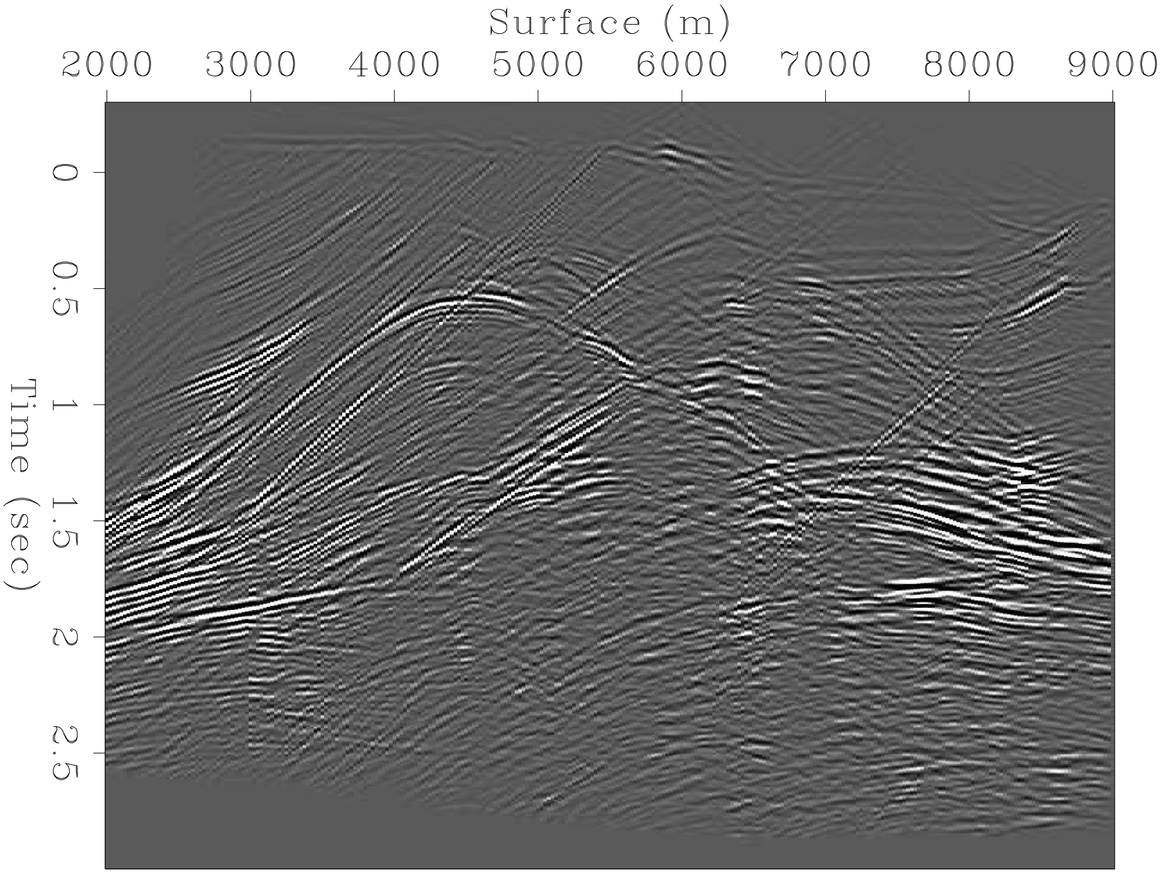

FIG. 2.15. Wave-stacked section of Marmousi data set with synthesis operator shown in Figure 2.14. wfsyn-marm-stk-pos-2 [CR]

is readily interpretable in terms of an angle-dependent reflectivity of the reflectors where the plane-wave is synthesized, since we can easily calculate the incidence angle to reflector from the angle of synthesized plane-wave and the dip of reflector.

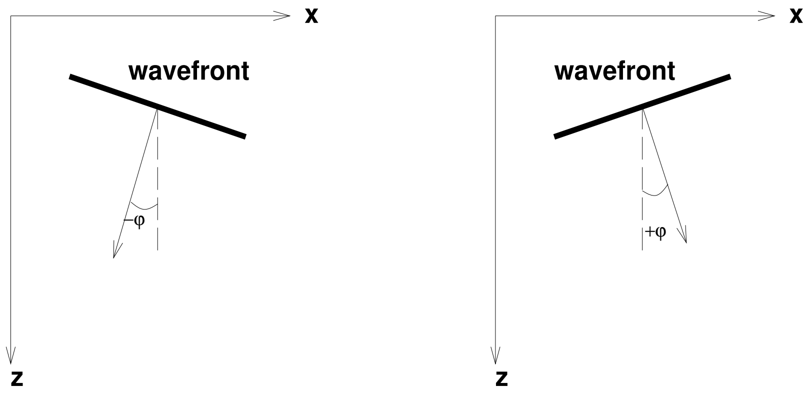

FIG. 2.16. The sign convention used in this thesis for the slanted plane wavefront. wfsyn-anglesign [NR]

2.4 Imaging the synthesized stack

After the wavefront synthesis, the synthesized stack is expressed as equation (2.4), and if we write it with a full operator, it becomes

$$\bar{\mathbf{g}}(z_0) = \sum_{n=1}^{N} W(z_0, z_n) R(z_n) W(z_n, z_0) \bar{\mathbf{s}}(z_0). \tag{2.14}$$

We can notice that this equation has the same form as the forward model of a shot record (equation (2.1)). Therefore, the imaging is performed in the same manner as profile imaging (Claerbout, 1985), with $\bar{\mathbf{g}}(z_0)$ as the upcoming wave and $\bar{\mathbf{s}}(z_0)$ as the downgoing wave. According to the profile imaging concept, the reflectors exist in the earth at places where the downgoing wave is time-coincident with an upcoming wave (Claerbout, 1985). It can be explained by two procedures: extrapolation and imaging.

By recalling that the extrapolation operator is unitary, after extrapolating the upcoming and downgoing wavefield recursively, we have

$$W^*(z_m, z_0)\bar{\mathbf{g}}(z_0) = R(z_m) W(z_m, z_0) \bar{\mathbf{s}}(z_0) \tag{2.15}$$

where $*$ denotes the adjoint. For each depth level, extrapolation is performed as follows:

$$\bar{\mathbf{g}}(z_n) = W^*(z_n, z_m)\bar{\mathbf{g}}(z_m) \tag{2.16}$$

and

$$\bar{\mathbf{s}}(z_n) = W(z_n, z_m)\bar{\mathbf{s}}(z_m). \tag{2.17}$$

The upcoming waves are extrapolated backward in time, the downgoing waves, forward in time. Keeping in mind that the upcoming wavefield is the convolution of the reflectivity with the downgoing wave field, we can obtain the reflection coefficient from equations (2.16) and (2.17) by deconvolving $\bar{\mathbf{s}}(z)$ from $\bar{\mathbf{g}}(z)$ as follows:

$$R(z_n) = \sum_{\omega} \frac{\bar{\mathbf{g}}(z_n)\bar{\mathbf{s}}^*(z_n)}{\bar{\mathbf{s}}(z_n)\bar{\mathbf{s}}^*(z_n) + \epsilon^2}. \tag{2.18}$$

In equation (2.18), ϵ^2 represents a small positive value that is introduced for stability because $\bar{\mathbf{s}}(z_n)$ may contain zeros, and the summation of all frequency components is equivalent to inverse Fourier transforming and takes the zero-time component.

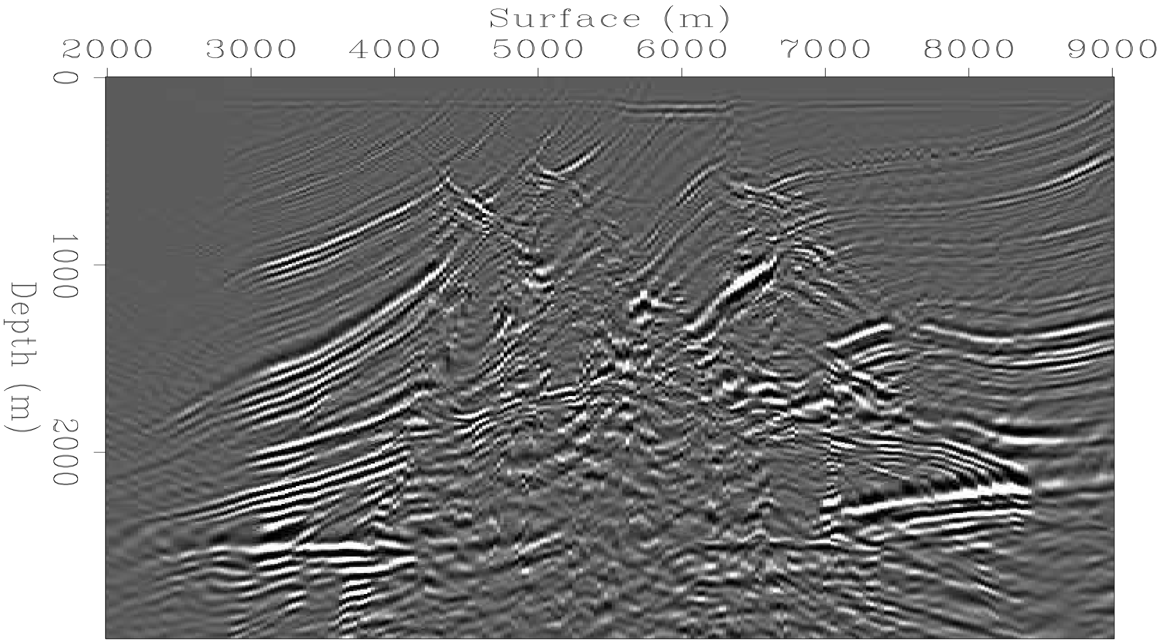

FIG. 2.17. Image obtained by synthesizing a plane-wave with $p = 0(s/m)$ at surface. wfsyn-pws-mar-pln-0 [CR]

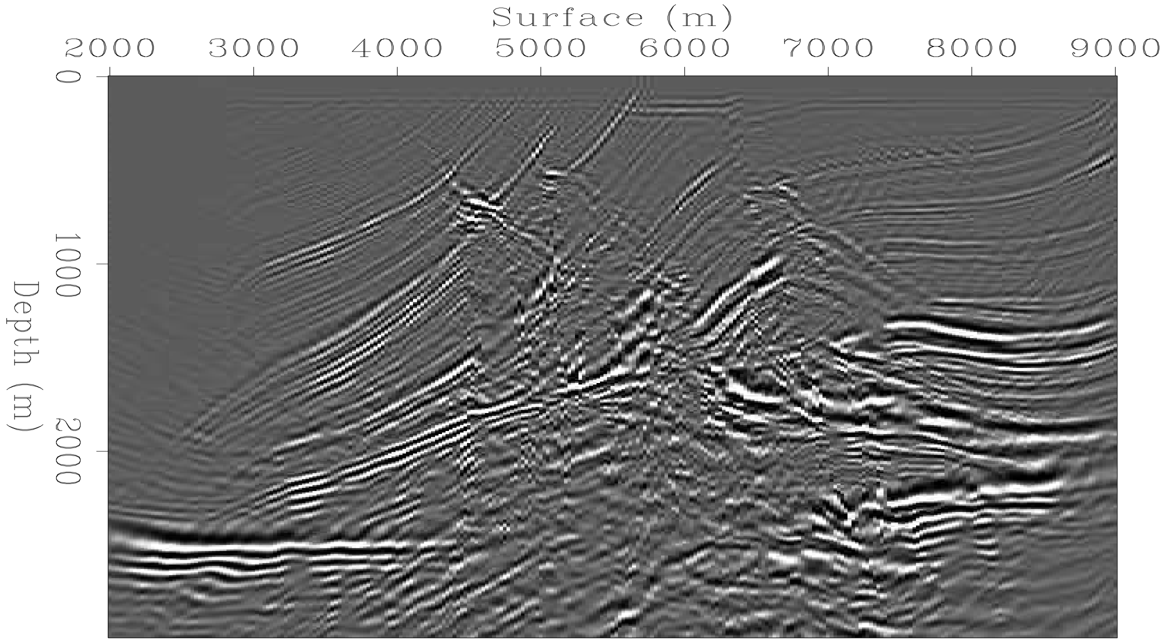

FIG. 2.18. Image obtained by synthesizing a plane-wave with $p = .0001(s/m)$ at surface. wfsyn-pws-mar-pos-0 [CR]

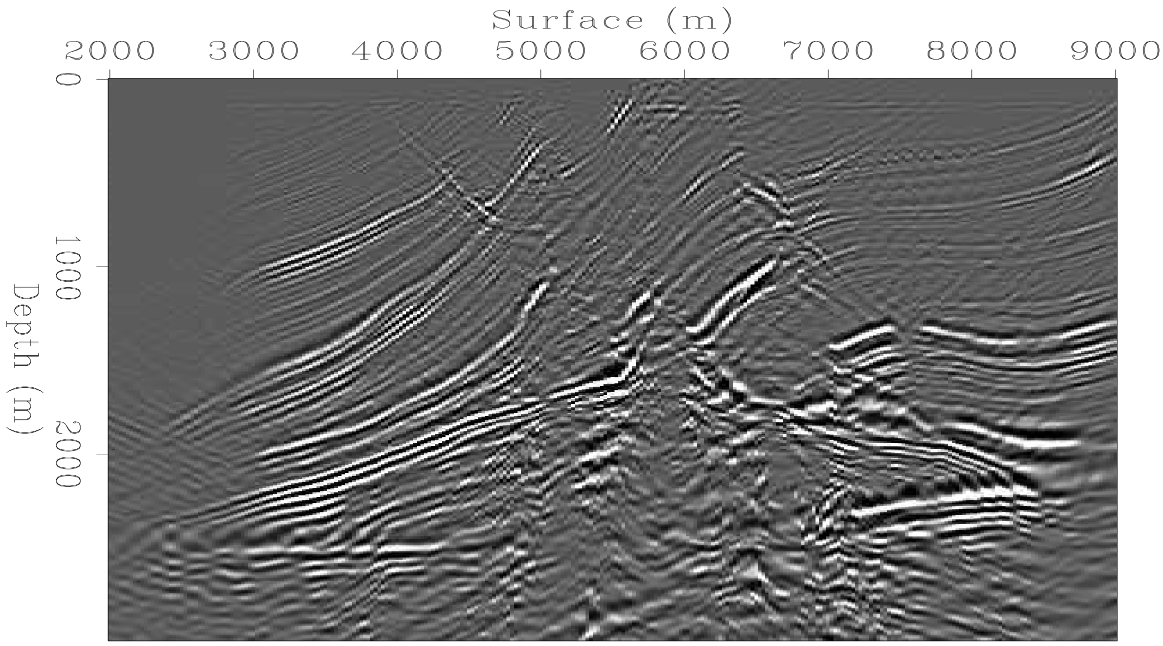

FIG. 2.19. Image obtained by synthesizing a plane-wave with $p = 0(s/m)$ at 1200m depth. wfsyn-pws-mar-pln-1 [CR]

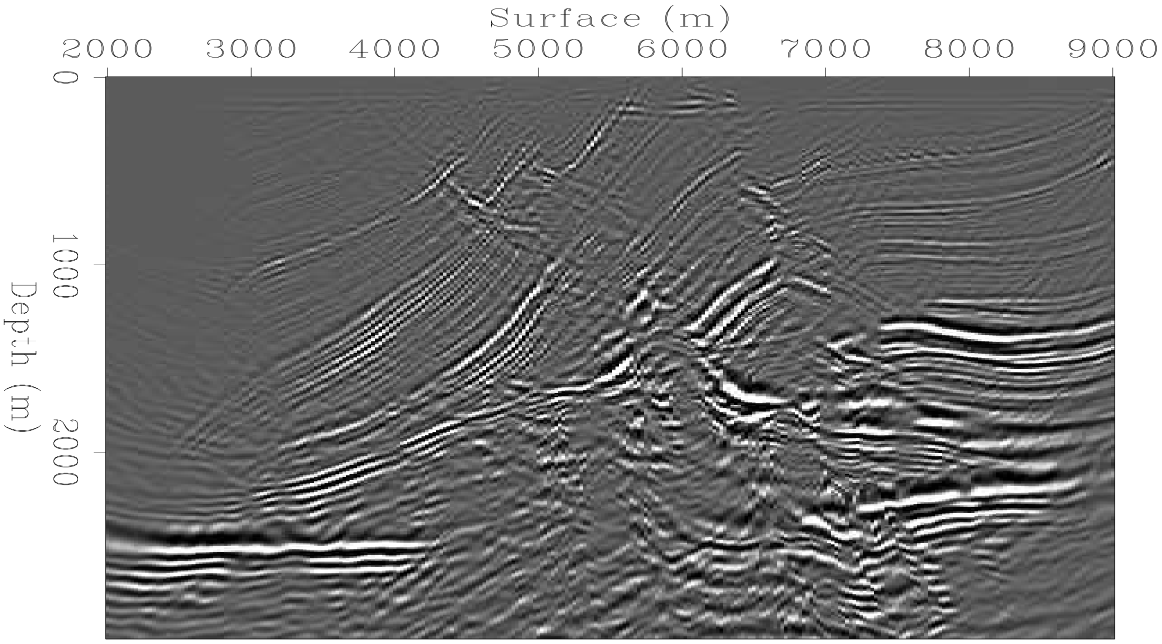

FIG. 2.20. Image obtained by synthesizing a plane-wave with $p = .0001(s/m)$ at $1200m$ depth. wfsyn-pws-mar-pos-1 [CR]

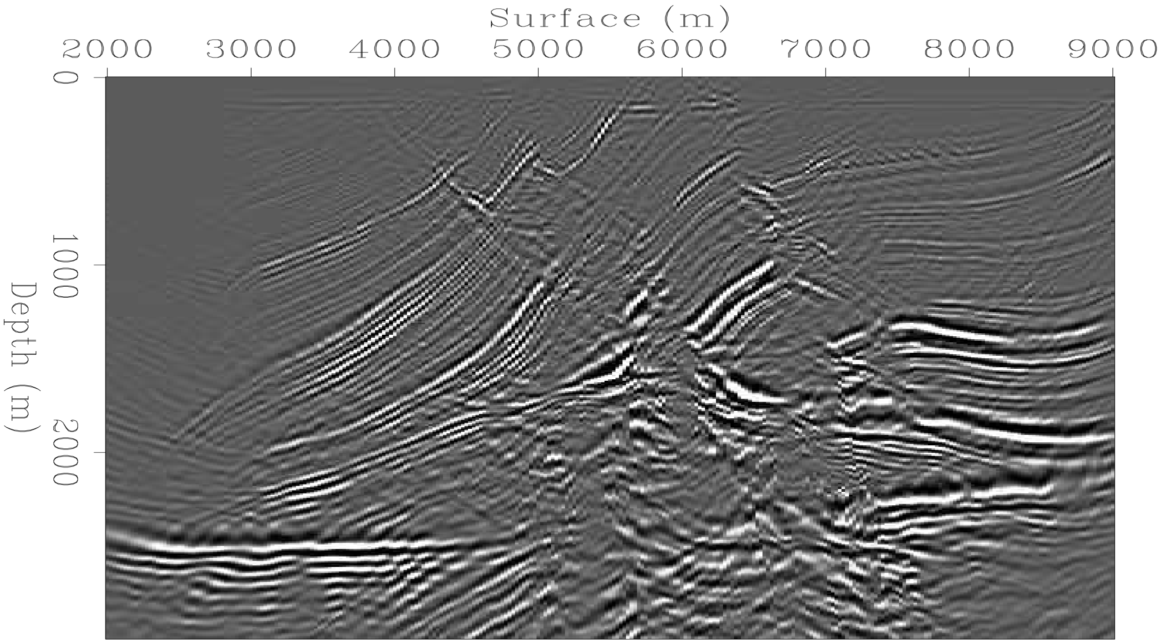

FIG. 2.21. Image obtained by synthesizing a plane-wave with 10 degrees angle at $1200m$ depth. wfsyn-pws-mar-pos-2 [CR]

2.5 Image stacking versus patching

The images obtained by synthesizing plane waves can be handled in two ways, stacking or patching, according to the purpose of imaging. If one is interested in structure imaging, the stacking of all the images that were obtained by synthesizing different plane waves is helpful because it enhances the image quality by constructive interference where the reflector is and reduces noises by destructive interference. Figure 2.22 shows the result of image stacking with thirty-one plane waves synthesized at the surface, where the incidence angle changes from -30 degrees to 30 degrees. Comparing this to the image obtained by synthesizing a single plane-wave at the surface (Figure 2.17), we can see a significant improvement in the quality of reflector images.

On the other hand, if one is interested in the angle-dependent reflectivity recovery or prestack velocity estimation, each image obtained by synthesizing different plane waves should be saved separately because each image contains different information. Even in the image obtained by the synthesis of a plane-wave, only the portion of the image where the plane-wave was synthesized is interpretable because the plane-wave will be distorted after propagation through a complex velocity medium and we do not know the incidence angle of the distorted plane-wave at each depth unless we perform exhaustive ray-tracing. Therefore, I patched the interpretable parts of images obtained by synthesizing a plane-wave at different depths to produce common-incidence angle images. For example, Figure 2.23 shows the image obtained by patching twenty-one images obtained by synthesizing plane waves (0 degrees) at twenty-one equi-spaced depth levels. Comparing this to the image obtained by synthesizing a plane-wave at the surface (Figure 2.17), we can observe that the quality of images is almost the same in the entire section, unlike Figure 2.17, where the quality of image significantly changes from place to place.

2.6 Summary

The algorithm of plane wave synthesis (PWS) imaging is described in two steps; the synthesizing and the imaging. First a wavefront is synthesized by means of wave stack and then the imaging of the synthesized stack is performed like the conventional shot profile imaging.

The plane-wave synthesis along an irregular reflector can be achieved by means of wavefield datuming algorithm and will provide a fundamental framework for tomographic

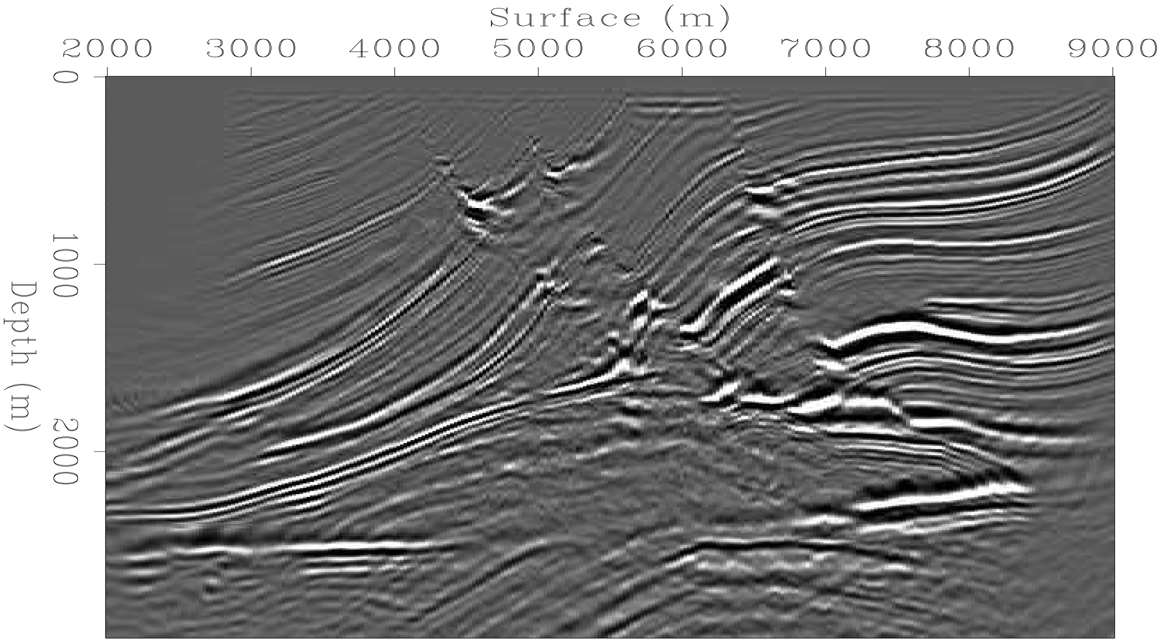

FIG. 2.22. Image obtained by stacking thirty-one plane wave synthesized at surface. Incidence angle at surface changes from -30 degrees to 30 degrees. wfsyn-pws-mar-stk-1 [CR]

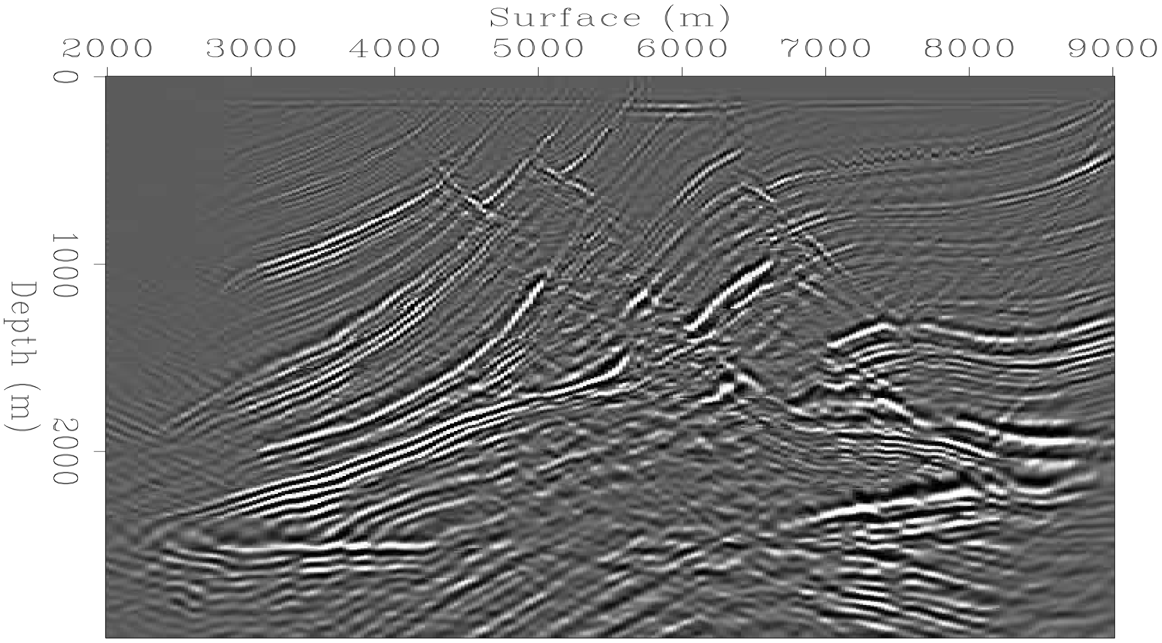

FIG. 2.23. Image obtained by patching twenty-one images which are obtained by synthesizing twenty-one plane waves which are equi-spaced in depth. wfsyn-pws-mar-pat-pln [CR]

velocity estimation explained in chapter 4. A common-incidence angle image section can be obtained by means of image patching after subsurface-oriented PWS imaging. It provides a useful framework for the angle-dependent reflectivity recovery explained in chapter 5.